

Electric-field effects in semiconductor quantum wells

Witold Trzeciakowski*

*Institute of Condensed Matter Theory, FORUM INFM, Department of Physics, University of Florence,
Largo Enrico Fermi 2, 50125 Florence, Italy*

Massimo Gurioli

*European Laboratory of Nonlinear Spectroscopy, Department of Physics, University of Florence,
Largo Enrico Fermi 2, 50125 Florence, Italy*

(Received 2 January 1991)

In the presence of an electric field the energy spectrum of a quantum well becomes continuous, with bound states transforming into resonances, but also with strong modifications in the above-barrier region. Analyzing the density of states (DOS) of the system, we find modulated oscillations of this quantity due to interference of the waves reflected from the well boundaries and from the slope of the electric-field potential. We show that these oscillations in DOS are related to the Fowler-Nordheim resonances in transmission through a double-barrier tunneling structure. We also calculate the absorption $\alpha(\hbar\omega)$ from the ground state in the well to the energy continuum above the barriers. We find a pronounced electric-field effect on $\alpha(\hbar\omega)$; the slowly varying curve for zero field transforms into a series of sharp peaks. The observation of these peaks requires narrow wells, wide barriers, and moderate electric fields. It would allow for the determination of important parameters like band offset or the value of the internal electric field.

I. INTRODUCTION

Progress in the physics of semiconductor heterostructures has been stimulated by their numerous applications: quantum-well lasers, high-speed transistors, resonant-tunneling diodes, etc. In most of these devices the electric field can be very strong, due to their small dimensions, e.g., the potential drop across a single quantum well can easily exceed the depth of the well. The electric field is also useful as a parameter allowing for the continuous tuning of the energy levels, for the modification of the selection rules for optical transitions, etc.

In the presence of a uniform electric field (of infinite range) the spectrum of any heterostructure becomes continuous, with bound states transforming into resonances of finite energy width. However, the first calculations of the energy spectrum in the presence of the field assumed that the levels remain discrete.^{1,2} Since then the broadening of the energy levels has been included perturbatively,³ i.e., assuming that the coupling between bound states and continuum is weak.

The most complete analysis of the continuous energy spectrum of single⁴ and multiple⁵ quantum wells has been performed by Austin and Jaros, who analyzed the density of states (DOS) without any assumptions about the coupling between the bound levels and the continuum. The following dispute in the literature⁶ arose because of the differences between approximate methods and the exact calculation in the high-field range. All these calculations have concentrated on the energy spectrum inside the quantum well, or only slightly above.

In the present paper we study the full spectrum of the quantum well in the presence of the field. We analyze the

change in DOS introduced by the well $\Delta\rho(E)$, using a simple and exact method for evaluating this quantity. In the energy range above the barriers we find interesting oscillatory structures in $\Delta\rho(E)$ that could not be obtained with perturbative methods. We also study the transmission across the double-barrier structure at higher energies and the absorption from the ground state in the well to the continuum above the barriers. Both of these quantities reveal very interesting electric-field effects, consistent with the structures found in $\Delta\rho(E)$.

We assume a uniform effective mass m^* throughout the heterostructure. In this case the boundary conditions for the envelope function and its gradient can be taken as continuity. For equal masses in the parabolic bands of the well and of the barrier material the eigenvalue problem becomes strictly one dimensional. We did not want to complicate the issue with the speculations about the boundary conditions,⁷ although the wave function in the presence of the field can be quite sensitive to them.⁸

We neglect the band-structure effects,⁹ i.e., the presence of X or L minima in the conduction band of the well and barrier material. As shown in Ref. 9 the Γ - X mixing induced by the field could be important only at very high fields (above 500 kV/cm for a single quantum well) while the effects we describe occur at much lower fields (of the order of 10 kV/cm). Of course at energies high above the Γ barriers the X minima come into play even at zero field. Therefore our calculations are valid in a limited energy range above the barriers (say, 0.2 eV for $\text{Al}_{0.3}\text{Ga}_{0.7}\text{As}$ barriers).

The paper is organized as follows. In Sec. II we briefly describe our method of determining $\Delta\rho(E)$ and we analyze this quantity for a single quantum well in the pres-

ence of the electric field. For the energy range inside the well we determine the positions and the widths of resonances, in agreement with previous calculations.⁴ In the energy range above the barriers we study the oscillatory structure in $\Delta\rho(E)$ and its dependence on the field and on the well parameters. Section III is devoted to the study of transmission $T(E)$ for a double-barrier structure and of the correspondence between the resonances in $T(E)$ and the oscillations in $\Delta\rho(E)$. In Sec. IV we evaluate the absorption from the ground state in the well to the continuum. We point out the most favorable conditions for the observation of the predicted effects. Section V contains the summary of our results.

II. DENSITY OF STATES IN THE CONTINUOUS SPECTRUM

The DOS of a quantum system is defined as

$$\rho(E) = \sum_n \delta(E - E_n), \quad (1)$$

while the local density of states (LDOS), used by some authors¹⁰⁻¹² may be defined as

$$\begin{aligned} \rho_\Omega(E) &= \int_\Omega dz \sum_n |\Psi(E_n, z)|^2 \delta(E - E_n) \\ &= \int_\Omega dz |\Psi(E, z)|^2 \rho(E). \end{aligned} \quad (2)$$

Here $\{E_n\}$ are the eigenvalues of the system, $\Psi(E_n, z)$ are the corresponding wave functions, and Ω is some selected region of integration. For Ω being the whole space we obtain the DOS defined in Eq. (1).

We consider a finite (but big) system so that the energy spectrum is discrete (but dense). As we show at the end of this section, the use of the LDOS can be misleading because it depends on the integration region Ω . Instead, we analyze the change in DOS $\Delta\rho(E)$ introduced by the considered structure¹³ (e.g., by the quantum well),

$$\Delta\rho(E) = \rho(E) - \rho_0(E), \quad (3)$$

where $\rho_0(E)$ is the DOS in a big "box" and $\rho(E)$ is the DOS in the same box with the structure. The choice of the box is irrelevant except that it has to be sufficiently big so that $\Delta\rho(E) \ll \rho_0(E)$. For the zero-field case it is often convenient to take the big box as a wide quantum well with infinite barriers, for the structures with the electric field it is natural to choose the triangular box, i.e., an infinite barrier at $z=0$ and a linear potential elsewhere. Suppose that the condition for the energy levels in an empty box is

$$D_0(E_n^0) = 0, \quad (4)$$

and for the box with the structure,

$$D(E_n) = 0. \quad (5)$$

The functions $D_0(E)$ and $D(E)$ are obtained by solving the set of boundary conditions for the wave function and its gradient. The DOS is then given by the inverse of the spacing between the levels,

$$\rho_0(E_n^0) = \frac{1}{\Delta_n^0}, \quad (6)$$

$$\rho(E_n) = \frac{1}{\Delta_n}, \quad (7)$$

where $\Delta_n^0 = E_{n+1}^0 - E_n^0$ and $\Delta_n = E_{n+1} - E_n$. Both of these densities increase with the box size. However, the difference between them, which characterizes the considered structure, stays finite even for an infinite box. Thus we can write

$$\Delta_n = \Delta_n^0 + x_n, \quad (8)$$

with $|x_n| \ll \Delta_n^0$. The change in DOS becomes

$$\Delta\rho(E_n) \cong -\frac{x_n}{(\Delta_n^0)^2}. \quad (9)$$

The shift in the energy spacing can be obtained by expanding $D(E)$ around $E_n + \Delta_n^0$, and we finally obtain

$$\Delta\rho(E_n) \cong \frac{1}{(\Delta_n^0)^2} \frac{D(E_n + \Delta_n^0)}{D'(E_n + \Delta_n^0)}, \quad (10)$$

where $D'(E)$ is the first derivative of $D(E)$. Thus, knowing the eigenvalue conditions (4) and (5) we can determine $\Delta\rho(E)$ from Eq. (10).

So far we have considered the one-dimensional (1D) system. In any heterostructure we also have the free motion in the directions parallel to the interfaces. Therefore every level of our 1D structure introduces in fact a steplike DOS. The full DOS for a given energy E is the sum of such steps for all lower-lying levels $E_n < E$. For the energy E in the continuum this sum becomes the integral of 1D DOS plus the constant contribution from all lower-lying bound states. We prefer to consider the 1D DOS but it would be straightforward to integrate it. Also, the absorption discussed in Sec. IV contains the 1D DOS due to the wave-vector conservation in optical transitions.

Let us now apply this method to the quantum well of depth V_0 and width L , subject to a uniform electric field F . The natural choice of the big box is the triangular potential shown in Fig. 1. The increase in the box size is achieved by increasing X . The condition for the energy levels in an empty box is given by Eq. (4) with

$$D_0(E) = \text{Ai}(y_0), \quad (11)$$

where Ai is the Airy function¹⁴ and

$$y_z = \left[\frac{2m^*eF}{\hbar^2} \right]^{1/3} \left[z - \frac{E}{eF} \right], \quad (12)$$

so that $y_0 = -(2m^*eF/\hbar^2)^{1/3}E/eF$. For the box with the well,

$$D(E) = \alpha_1 \text{Ai}(y_0) + \beta_1 \text{Bi}(y_0), \quad (13)$$

where α_1 and β_1 are given by lengthy expressions obtained from the boundary conditions at $z=X$ and $z=X+L$. For a big box (i.e., large X) we can use the asymptotic formulas¹⁴ for Ai(y_0) and Bi(y_0). This yields

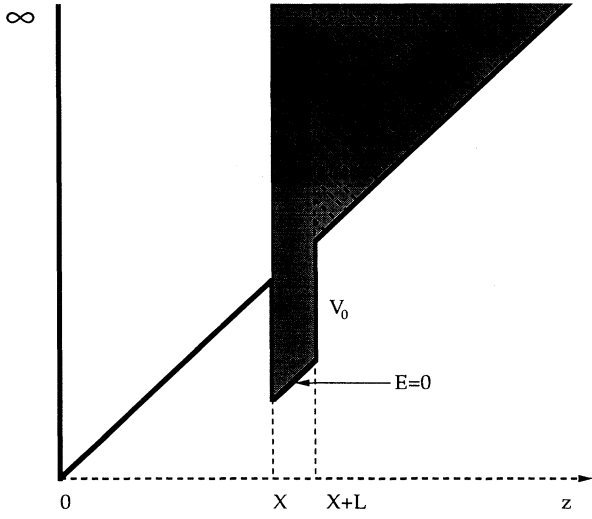


FIG. 1. Potential profile used for the determination of DOS. The arrow shows the energy reference used in $\Delta\rho(E)$ figures—the middle of the well bottom.

the following expression for the energy levels in a triangular box:

$$E_n^0 \cong \left[\frac{3\pi n e F}{2} \left(\frac{\hbar^2}{2m^*} \right)^{1/2} \right]^{2/3}, \quad n \gg 1, \quad (14)$$

so that the DOS $\rho_0(E) \propto \sqrt{E}$. However, for some more complicated structures than the triangular box the expression for $D_0(E)$ may be more complex so that the roots cannot be found analytically. The general procedure is therefore as follows: first we find two roots of $D_0(E)$ and the spacing between them, together with one root of $D(E)$. For a big box the spacing of the roots changes very slowly so that all subsequent roots of $D_0(E)$ and $D(E)$ can be found by linear interpolation. The size of the big box does not affect $\Delta\rho(E)$ but in the energy regions where we expect very narrow resonances it is necessary to increase X to get a better resolution.

Let us now look at the results of the calculation: first, the resonances in $\Delta\rho(E)$ originating from bound states at $F=0$. Figure 2 shows the broadening (and shift) of the ground state in a 30-Å, 70-meV quantum well for $m^*=0.45m_0$ (heavy holes in GaAs); the energies are measured from the middle of the well bottom. We show this figure to demonstrate that our results for $\Delta\rho(E)$ coincide¹⁵ with those of Austin and Jaros, who presented a similar graph in Ref. 4. In Fig. 3 we show the evolution of three bound states in a wider well and the increase of their half-widths with the field. The excited levels behave nonmonotonically when the field is increased, as shown in Ref. 2 for an infinite well.

The results could be plotted in dimensionless units (energy in $E_0 = \hbar^2/2m^*L^2$; field in $F_0 = E_0/eL$) so that they apply both for electrons and for holes. However, the situation for the holes is more complicated because for the in-plane k vectors different from zero, the heavy- and

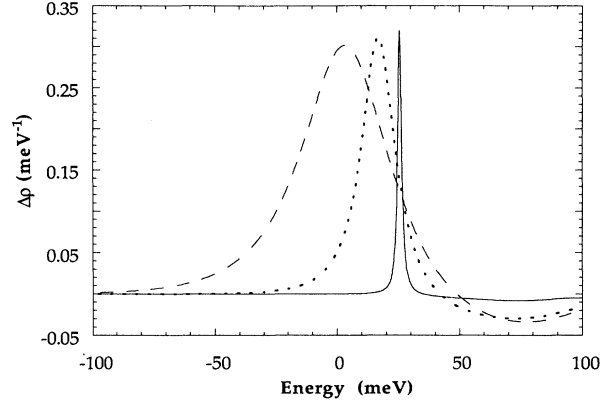


FIG. 2. Quasibound state in a 30-Å, 70-meV quantum well for heavy holes ($m^*=0.45m_0$) at three different fields: 100 kV/cm (solid line), 240 kV/cm (dotted line: $\Delta\rho$ multiplied by 9), 440 kV/cm (dashed line: $\Delta\rho$ multiplied by 27).

light-hole states become coupled and the calculation should be done for a 4×4 (or 6×6) Luttinger Hamiltonian (as in Ref. 16). Therefore in the following we shall concentrate on the electrons ($m^*=0.067m_0$ in the well and in the barriers) and we shall use ordinary units.

Figure 4(a) shows $\Delta\rho(E)$ in a wide energy range¹⁷ for a 100-Å, 100-meV well at the field of 20 kV/cm. At lower energies we can see two resonances originating from bound states at zero field. At energies above the upper barrier an oscillatory structure begins with slow

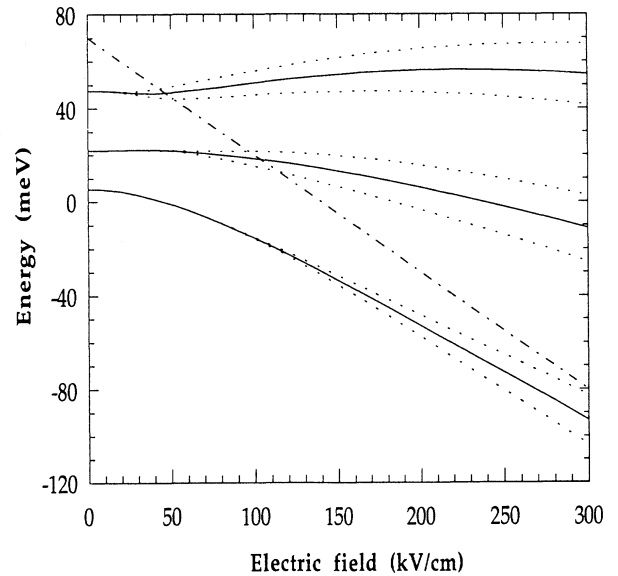


FIG. 3. Electric-field variation of three quasibound states in a 100-Å, 70-meV quantum well for heavy holes. Solid lines follow the position of DOS maxima, dots indicate the half-widths. The dashed-dotted line gives the position of the lower barrier edge.

modulation of the amplitude. The period of the fast oscillation increases with the field [Fig. 4(b)] while the slow modulation depends only on the width of the well. The number of nodes in a given energy region turns out to be proportional to the well width, i.e., if we triple the width, the number of nodes will triple. This resembles the condition for the zero-field resonances above the well, namely $kL = n\pi$. We can therefore attribute the oscillatory structure in $\Delta\rho(E)$ to the reflections of the wave function from the well boundaries and from the slope of the electrostatic potential. If there was only one boundary, we would only get the fast component. Due to the interference of the wave functions reflected from two interfaces we get the slow modulation, which depends only on the well width.

The interpretation of the structures in the DOS becomes easier when we look at the wave functions corresponding to the maxima and the minima of $\Delta\rho(E)$. In Fig. 5 we plot the normalized wave functions corresponding to the energies of the first maxima [solid lines in Figs. 5(a) and 5(b)] and minima [solid lines in Figs. 5(c) and 5(d)] for a 100-Å, 100-meV well at the field of 10 kV/cm [$\Delta\rho(E)$ is shown in Fig. 6]. We can see that the wave functions approximately vanish at the right-hand-side interface (maxima) or at the left-hand-side interface (minima). Furthermore the comparison with the wave functions corresponding to the same energy value but for $V_0=0$ (dotted lines in Fig. 5) shows that the maxima (minima) in $\Delta\rho(E)$ correspond to an increase (decrease) of the probability in the right-hand-side barrier region. When the wave function vanishes at both interfaces we get the node in $\Delta\rho(E)$ at the corresponding energy and no change of the wave function in the right-hand-side barrier region [Fig. 5(e)]. This supports the interpretation given above. It also means that the maxima of $\Delta\rho(E)$ correspond to bound states in a triangular well starting at the right-hand-side boundary (dashed region in Fig. 1) and the minima are related to bound states in the potential starting at the left-hand-side boundary (shaded region in Fig. 1). This is illustrated in Fig. 6 where the arrows denote the energies of bound states in the two potentials mentioned above. The node in $\Delta\rho(E)$ occurs when the arrows corresponding to the two potentials become aligned. The condition for the node \tilde{E}_n can be derived from the asymptotic formulas for the Airy functions

$$\tilde{E}_n = \frac{(\hbar n \pi)^2}{2m^*L^2}, \quad (15)$$

which coincides with the zero-field resonance condition $kL = n\pi$. For higher energies the Airy functions in the well resemble trigonometric functions—the well bottom seems flat from high above.

It is interesting to study the low-field limit of the structures in $\Delta\rho(E)$. In Fig. 7 we show the comparison between $\Delta\rho(E)$ for a 40-Å, 200-meV well for $F=0$ (dashed line) and $F=1$ kV/cm (solid line). We have checked that the dashed line, which is close to zero in the considered energy region, represents the average of the solid one. The electric-field effect resembles the magnetic-field effect: the average DOS for small fields

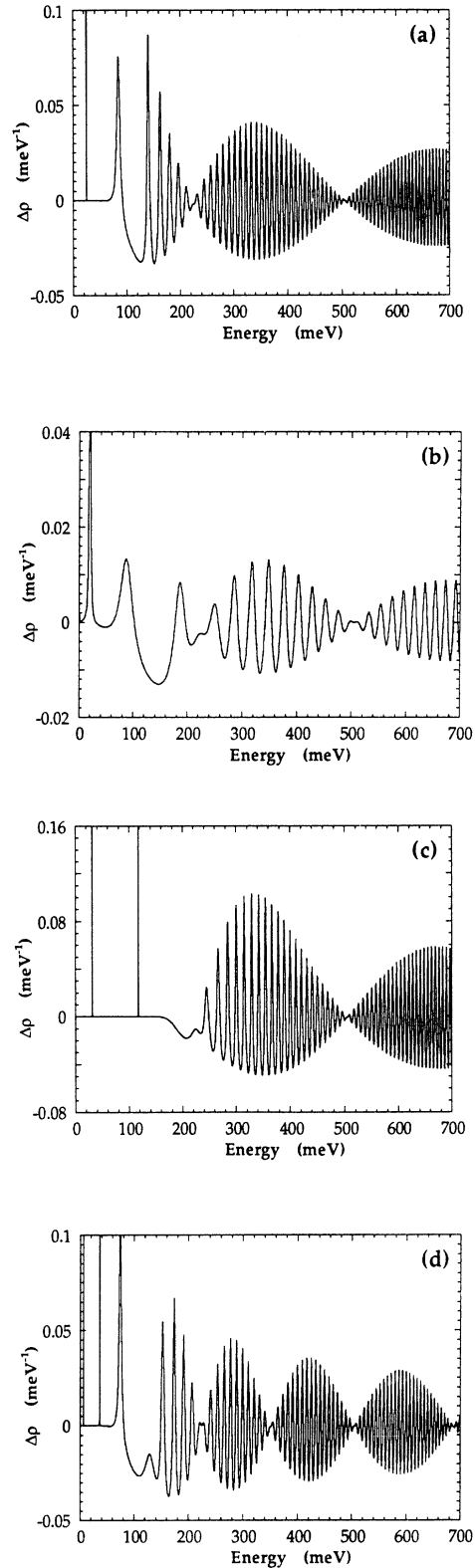


FIG. 4. Change in DOS for electrons ($m^*=0.067m_0$) introduced by the well: (a) 100-Å, 100-meV well at $F=20$ kV/cm; (b) 100-Å, 100-meV well at $F=60$ kV/cm; (c) 100-Å, 200-meV well at $F=20$ kV/cm; (d) 200-Å, 100-meV well at $F=20$ kV/cm.

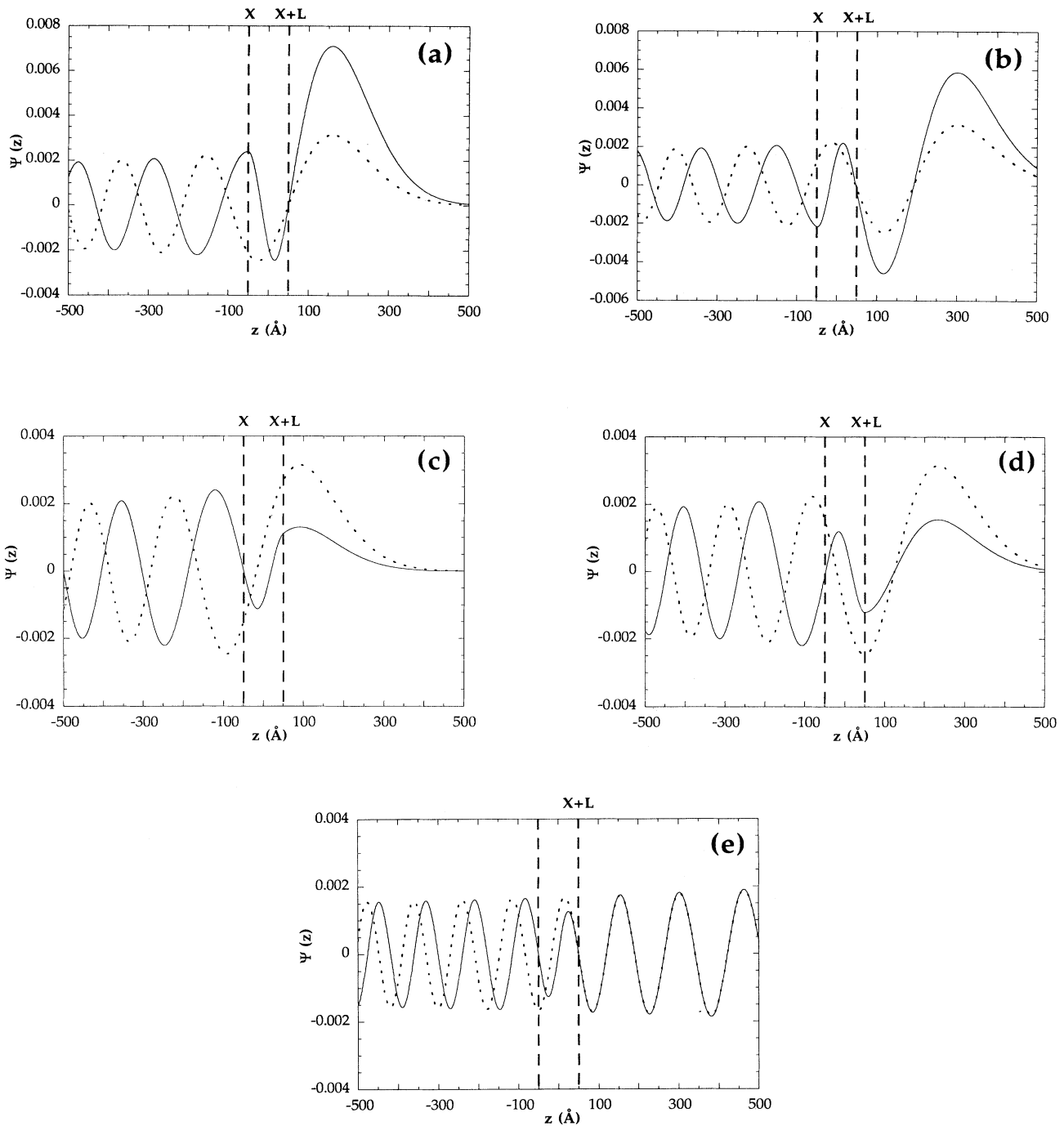


FIG. 5. Wave functions at different energies for a 100-Å, 100-meV well at $F=10$ kV/cm (solid lines). Dotted lines denote the wave functions for $V_0=0$ (no well) at same energies. The well region is between the dashed lines. The energies correspond to the first two maxima of $\Delta\rho(E)$: (a) $E=124.4$ meV, (b) $E=138.6$ meV; the first two minima of $\Delta\rho(E)$: (c) $E=117.6$ meV, (d) $E=131.8$ meV; the node in $\Delta\rho(E)$: (e) $E=225.3$ meV. Note in (e) that the wave functions coincide in the right-hand-side barrier region. The corresponding $\Delta\rho(E)$ is shown in Fig. 6.

tends to the zero-field case but locally $\Delta\rho(E)$ (even for a very small field) turns out to be qualitatively different. Of course our calculation is not realistic for very small fields because it assumes coherent wave functions over a large

region of the sample. At weak fields the reflection from the slope of the electrostatic potential occurs far away from the quantum well.

Finally let us briefly discuss the local density of states,

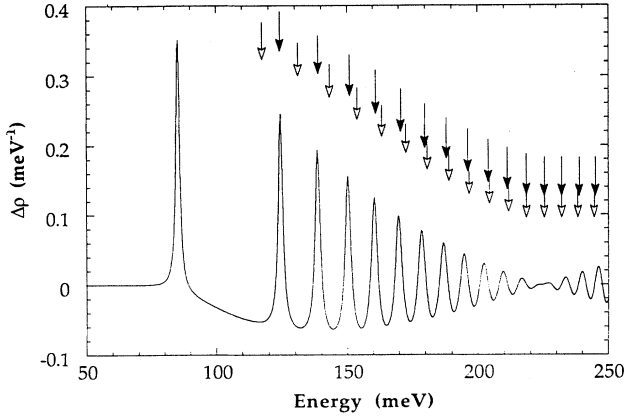


FIG. 6. Change in DOS introduced by a 100-Å, 100-meV well at 10 kV/cm. Black (white) arrows denote the positions of bound states in the dashed (shaded) potential regions of Fig. 1.

as defined in Eq. (2). It is often believed^{10–12} that the study of quantum-well resonances can be performed using this quantity, with the integration volume Ω taken as the region of the well ($X \leq z \leq X + L$). Therefore, for the case of the 100-Å, 100-meV, 10-kV/cm structure (like in Figs. 5 and 6) we compare in Fig. 8 the local density of states, evaluated¹⁸ for two choices of Ω : the quantum-well region [$\rho_W(E)$, solid line] or the right-hand-side barrier region [$\rho_B(E)$, dotted line]. We can see that the results are very different for the two regions and in both cases $\rho_\Omega(E)$ does not coincide with $\Delta\rho(E)$ (plotted in Fig. 6). In Fig. 8 we clearly see the modulated oscillations of $\rho_B(E)$ in the higher-energy region (around its value for $V_0=0$), but only small peaks corresponding to quasi-bound states in the well. These peaks are much more pronounced in $\rho_W(E)$ which, in turn, only shows a small and not modulated oscillatory structure at high energy.

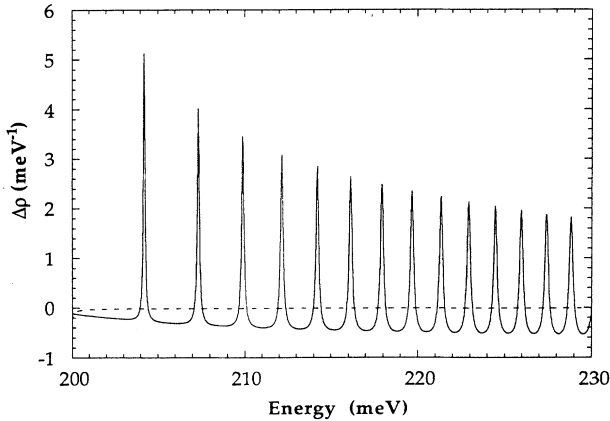


FIG. 7. Change in DOS due to a 40-Å, 200-meV well at $F=1$ kV/cm (solid line) and at $F=0$ (dashed line).

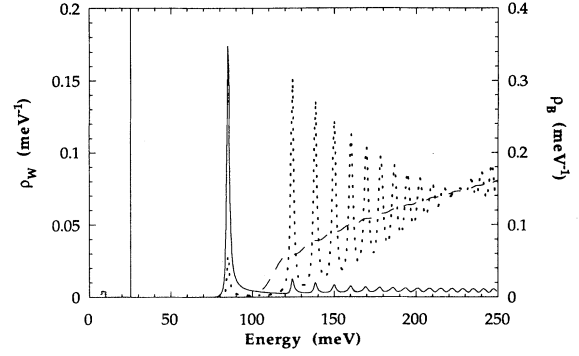


FIG. 8. Local DOS calculated for the well region (solid line) and for the barrier region (dotted line). The dashed line is the local DOS in the barrier for $V_0=0$ (no well).

This shows that LDOS is not equivalent to DOS and that it strongly depends on the choice of the region Ω .

III. TRANSMISSION RESONANCES

It is interesting to see how the oscillatory structure in $\Delta\rho(E)$ affects the transmission above a quantum well. Of course, in order to have a nonzero transmission we have to consider a structure different from the well in a semi-infinite linear potential; let us consider a double barrier, shown in Fig. 9. This structure introduces two additional interfaces, complicating the picture considered in the previous section. We also realize that the oscillatory behavior of $\Delta\rho(E)$ was due to the reflection from the potential slope above the well. However, in order to have strong

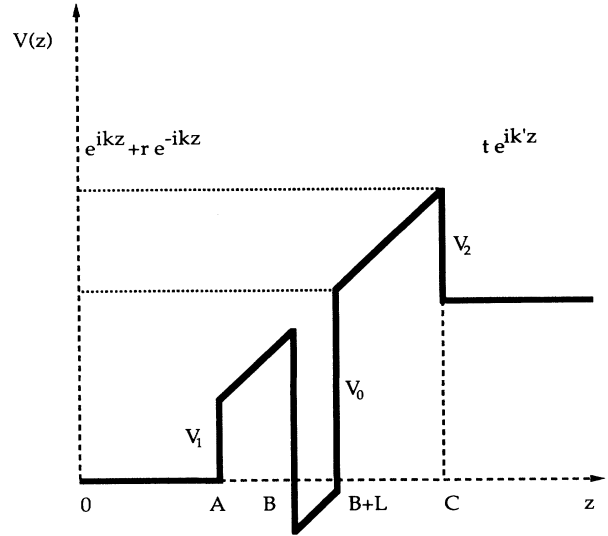


FIG. 9. Potential profile of the double-barrier structure containing the quantum well of depth V_0 and width L in the electric field of finite range. The wave functions in the two flat potential regions are displayed. The transmission is given by $|t|^2 k'/k$. The energies are measured from the upper flat region.

reflection from the potential slope the transmission must be weak.

In spite of all these limitations, it is possible to see in transmission the effects we found in $\Delta\rho(E)$. We have calculated analytically the transmission for the potential profile shown in Fig. 9. As we are mainly interested in the energy region marked by the dotted lines in Fig. 9 (this is where we expect to see the oscillatory structure) we had to use wide right-hand-side barrier to study a wide energy region.

In Fig. 10(a) we show (solid line in a semilogarithmic scale) the transmission probability $T(E)=|t(E)|^2k'/k$ (the symbols refer to Fig. 9) across a 100-Å, 250-meV, quantum well at $F=10$ kV/cm. The barriers were 1000 Å wide and their height from outside was 100 meV (we choose $V_1=V_2$). On the same figure we show (dashed line in a linear scale) the corresponding $\Delta\rho(E)$. Maxima in transmission coincide with those in DOS, even if the structures in transmission are less pronounced being superimposed on a very steep slope. A similar comparison for a 280-meV, 200-Å well at 10 kV/cm [Fig. 10(b)] shows that the node in $\Delta\rho(E)$ is also present in transmission.

The transmission peaks, due to the levels in a triangu-

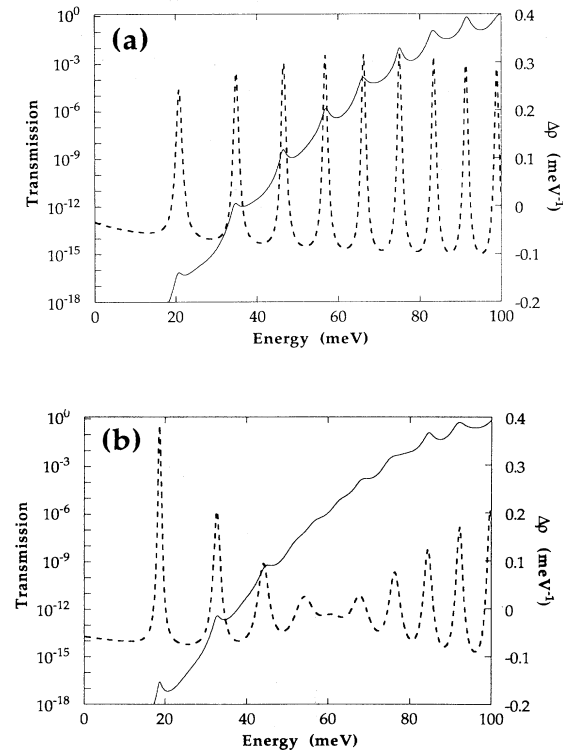


FIG. 10. Transmission coefficient (logarithmic scale, solid lines) and the change in DOS (linear scale, dashed lines) for the following parameters of the structure in Fig. 9: (a) $L=100$ Å, $V_0=250$ meV; (b) $L=200$ Å, $V_0=280$ meV. In both cases $F=10$ kV/cm, the barriers were 1000 Å wide and their height from outside was $V_2=V_1=100$ meV.

lar “well,” above the right-hand-side barrier are well known as the Fowler-Nordheim¹⁹ resonances and have been recently discussed in Ref. 20. Here we show, however, that in a double-barrier structure we have strong interference effects due to the second interface of the well. This interference can enhance or destroy the transmission resonance as shown in Fig. 11 where we compare the transmission across two double-barrier structures with different well depths (solid and dashed lines). We can see that the presence of the well strongly modifies the amplitude of the Fowler-Nordheim peaks although their position (with respect to the upper barrier) depends only on the electric field. The transmission resonances discussed here are probably the source of conductance oscillations in the high-voltage region, reported in Ref. 21 for a multiple-quantum-well structure.

IV. ABSORPTION FROM THE GROUND STATE TO THE CONTINUUM

Another important quantity that could reveal the electric-field-induced oscillations is the absorption from

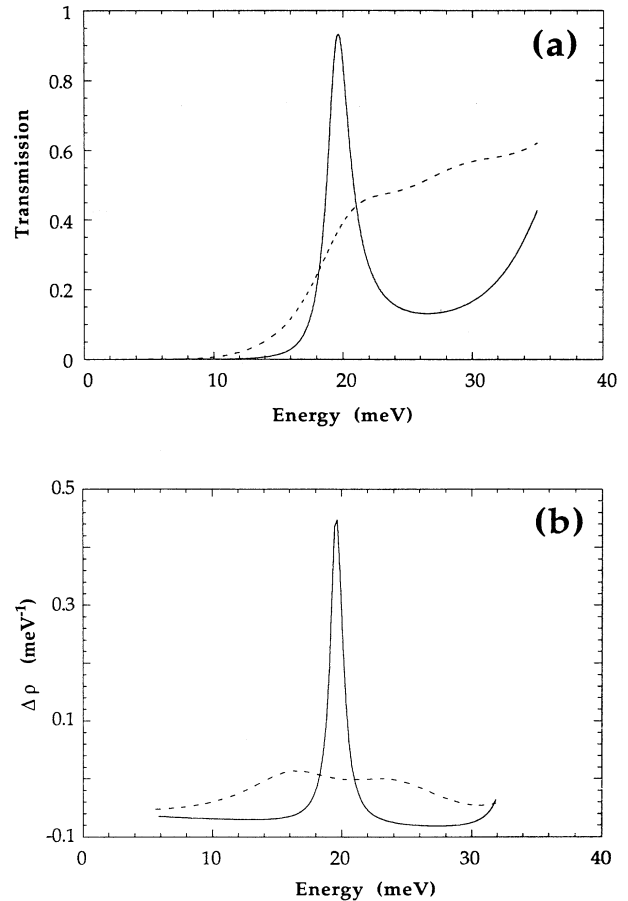


FIG. 11. The effect of the well parameters on (a) the transmission resonance and (b) on the corresponding $\Delta\rho(E)$ resonance. Solid lines are for $V_0=320$ meV, dashed lines for $V_0=250$ meV. In both cases $L=200$ Å, $F=10$ kV/cm, $V_2=V_1=30$ meV, and the barriers are 300 Å wide.

the ground state in the well to the continuum at higher energies. Several oscillatory optical effects are known in bulk semiconductors²² (Franz-Keldysh oscillations) and in superlattices²³ (Wannier-Stark ladders). Here we want to consider a new type of effect associated with the presence of the electric field and the boundaries of a single quantum well.

In order to deal with discrete initial state we consider the potential profile shown in Fig. 12, i.e., we assume a finite range of the electric field (the upper limit of the field is irrelevant). If we considered the potential profile of Fig. 1 we would face two problems: (i) we would have a continuum of initial states instead of the discrete ground state, and (ii) most of the wave functions of the initial states would be outside of the well, in a big box. For a linear potential these parts of the wave functions would give the dominant contribution to the absorption. This, in turn, would lead to the unphysical dependence of the absorption on the box size and the quantum-well contribution would be negligible.

All previous calculations of the infrared electroabsorption in quantum wells²⁴ were performed for discrete energy levels (including the field-dependent broadening phenomenologically). Here we evaluate the absorption to the continuum of states and we obtain all the structures in $\alpha(\hbar\omega)$ directly. Our calculation is valid for arbitrary field strength while the previous ones applied only to narrow Lorentzian resonances.

The momentum matrix element $\langle p_z \rangle$ between the ground state and an arbitrary "continuum" state can be determined analytically (see the Appendix) and the oscillator strength can be written as

$$f = \frac{2}{\hbar\omega m^*} |\langle p_z \rangle|^2. \quad (16)$$

Multiplying this by the density of final states we obtain

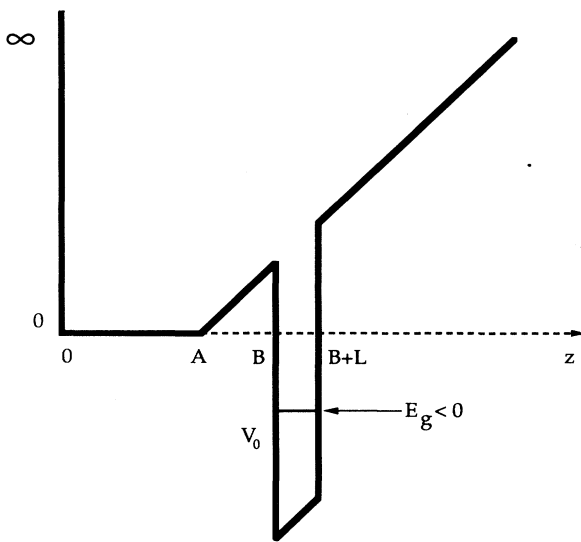


FIG. 12. Potential profile used for the absorption calculation. The ground state is bound while the continuum starts at $E=0$.

the absorption $\alpha(\hbar\omega)$ in arbitrary units. We also evaluated $\alpha(\hbar\omega)$ separately for the $F=0$ case.²⁵ In that case the box is flat and extends from $-A/2$ to $A/2$ and the well is placed in the middle. The transition from the symmetric ground state only takes place to the antisymmetric continuum states so that the absorption is "insensitive" to half of the excited states. This is qualitatively different from the $F \neq 0$ case.

Our calculation describes the absorption in a 1D system but it also applies to the real, 3D quantum well. The plane waves describing the motion parallel to the interfaces cancel in the momentum matrix element, i.e., the parallel wave vector is conserved. For parabolic dispersion all transitions from the ground subband to the excited continuum subband occur at the same energy $\hbar\omega$. Therefore the oscillator strength only has to be multiplied by the number of occupied states in the ground subband (assuming the continuum states are free). The summation over the final states thus involves only a one-dimensional density of states.

Let us now look at the results for the 60-Å, 250-meV well at $F=20$ kV/cm [Fig. 13(a)]. For these parameters of the well there are two bound states at $F=0$ and the huge absorption peak at 157 meV is due to the intersubband transition. At the energies above the top of the well

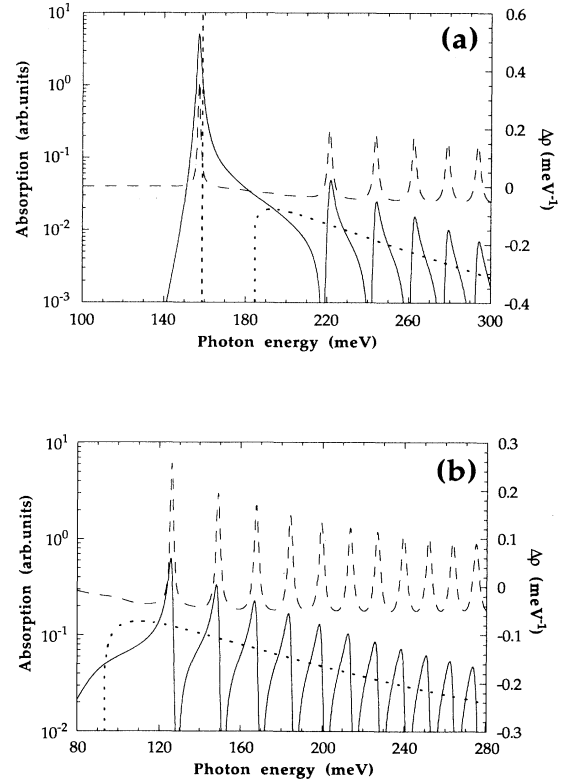


FIG. 13. Absorption (logarithmic scale, solid lines) and the change in DOS (linear scale, dashed lines) (a) for the 60-Å, 250-meV well at $F=20$ kV/cm and (b) for the 25-Å, 250-meV well also at $F=20$ kV/cm. The dotted line shows the zero-field absorption.

we can see multiple absorption peaks at the same position as the $\Delta\rho$ peaks. The correspondence between $\alpha(\hbar\omega)$ and $\Delta\rho$ is also clear in Fig. 13(b) where we plot these quantities for a 25-Å, 250-meV well also at $F=20$ kV/cm. In this case there is only one bound state in the well and the only peaks in the absorption (and in $\Delta\rho$) are those due to the above-well resonances. There is, however, an important difference between $\alpha(\hbar\omega)$ and $\Delta\rho$. It consists in the lack of slow modulation in the absorption, i.e., the nodes in $\Delta\rho$ are not present in $\alpha(\hbar\omega)$ (see Fig. 14). This is due to the fact that $\Delta\rho$ is related to the overall behavior of the eigenstates while $\alpha(\hbar\omega)$ monitors the wave functions' localization mainly in the well region. For this reason $\alpha(\hbar\omega)$ resembles somewhat the LDOS calculated for the well region (ρ_W in Fig. 8).

Figure 13 reveals another interesting property of $\alpha(\hbar\omega)$ (not present in $\Delta\rho$); the intensity of the above-barrier peaks is much higher for the narrow well than for the wide one. This feature of the absorption to the continuum is also present for $F=0$. It is a consequence of the f -sum rule; once the first excited state is pushed out of the well the intersubband transition disappears very quickly (Fig. 14) and the continuum transitions gain strength. As long as the excited state remains quasibound, it absorbs most of the oscillator strength and the multiple-peak structure at higher energies will be hard to see [Fig. 13(a)]. Let us therefore look at the narrow-well case again (Fig. 15). The electric-field effect on the absorption to the continuum is surprisingly strong [compared, e.g., with the effect on the intersubband transition—Fig. 13(a)]; the threshold for $F=0$ is replaced by a smooth increase and a slowly varying curve is replaced by a series of sharp peaks. The height of these peaks is only an order of magnitude lower than for the intersubband transition in Fig. 13(a) so they should be observable. The presence of the peaks is a particularly attractive feature of the $F\neq 0$ absorption because it should allow for the determination of the depth of the well (band offset), electric field, and other important parameters.

When the field is reduced, the peaks become denser and denser, the average of $\alpha(\hbar\omega)$ tends to the zero-field

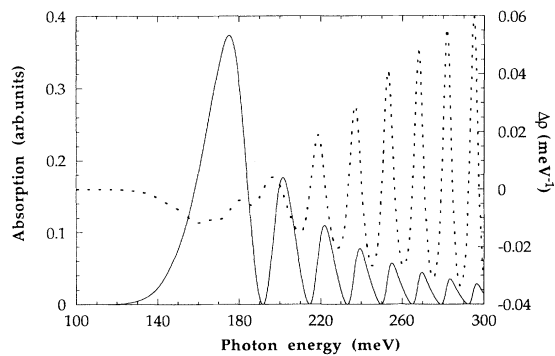


FIG. 14. Absorption for the 45-Å, 250-meV well at $F=20$ kV/cm (solid line) and the corresponding change in DOS (dotted line).

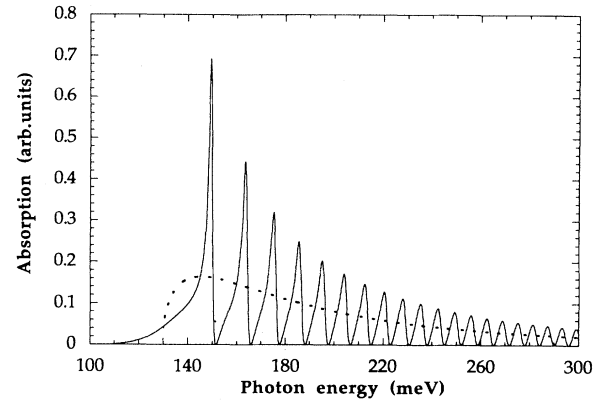


FIG. 15. Absorption for a 35-Å, 250-meV well at $F=0$ (dotted line) and at $F=10$ kV/cm (solid line).

absorption but locally even a small field changes $\alpha(\hbar\omega)$ dramatically. We have previously observed a similar behavior of $\Delta\rho$ (Fig. 7). The zero-field and the finite-field situations are qualitatively different. Of course our considerations are based on the idealized, coherent picture of the system; for weak fields our above-barrier states extend over large regions of the sample. For example, at $F=0.1$ kV/cm the first above-barrier resonance decays 1000 Å away from the well. Any scattering in this region will destroy the coherence and smear out the sharp resonance. In today's high-quality heterostructures the mean free path for the vertical transport can be as large as 0.5 μm (Ref. 21) but the absorption experiments are usually performed on multiple quantum wells where the barriers are at most a few hundred angstroms wide. Therefore, if we assume the 500-Å-wide barriers we can expect to see several peaks at $F\gtrsim 5$ kV/cm. Going to higher field increases their separation and lowers them (Fig. 16). We can see in Fig. 16 that the envelope of the peaks in $\alpha(\hbar\omega)$

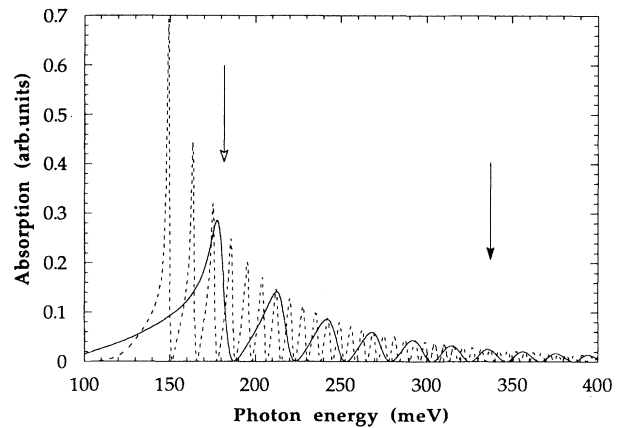


FIG. 16. Absorption for a 35-Å, 250-meV well at two different fields: 10 kV/cm (dashed line) and 40 kV/cm (solid line). The white (black) arrow denotes the potential energy 500 Å away from the right-hand-side interface for $F=10$ kV/cm ($F=40$ kV/cm).

is the same for different fields but at lower fields we deal with sharper and higher structures at lower energies. The arrows denote the energy values where the next well appears (for 500-Å barriers in a multiple-quantum-well structure), i.e., they mark the energy range where the peaks can be observable. It seems that for 500-Å barriers the optimal field would be around 10 kV/cm.

The most important sources of broadening would be the spread of the well parameters (in multiple-well samples) and the nonparabolicity, both the one induced by different masses in the well and in the barrier²⁶ and the one due to bulk nonparabolicity in the two materials. If the width of the intersubband peaks is about 10 meV (at low electric fields) we can expect our structures to be observable at the fields of a few kV/cm (and above).

The transitions to the continuum are very important for the infrared detectors based on the quantum-well structures.²⁷ Two multiple-quantum-well samples have been studied in Ref. 27: 45-Å wells with 140-Å $\text{Al}_{0.2}\text{Ga}_{0.8}\text{As}$ barriers and 40-Å wells with 300-Å $\text{Al}_{0.31}\text{Ga}_{0.69}\text{As}$ barriers. The second sample seems quite promising as far as the observation of the electric-field-induced structures is concerned. However, the zero-field absorption measured on this sample shows a broad low-energy edge which suggests that there may be some spread of the well depth in this 50-well sample. Such a spread could smear out the structures we predicted. It is also not clear whether or not the excited state is pushed out of the well in these samples—this depends critically on the band offset value (e.g., with 70/30 rule the excited state is still in the well). Further experimental studies are necessary, both because of the interesting physics of these phenomena and because of their potential application in infrared detectors.

V. SUMMARY AND CONCLUSIONS

We determined the change in DOS introduced by a single quantum well $\Delta\rho(E)$ in the presence of a uniform electric field F . In the energy region below the top of the well we obtained the energies and the widths of resonances originating from bound states at zero field. Our results coincide with those of earlier work.²⁻⁴ In the energy region above the top of the well we found modulated oscillations in $\Delta\rho(E)$ due to the reflections of the wave functions from the boundaries of the well and from the slope of the electrostatic potential. The modulation depends only on the well width while the fast oscillation is related to the bound states formed by the triangular potential above the barrier. We demonstrated that the use of the local density of states can be misleading as it strongly depends on the region under consideration.

We have then calculated the transmission $T(E)$ through the double-barrier tunneling structure (in the electric field) and we found that the peaks in $T(E)$ coincide with those in $\Delta\rho(E)$. The transmission maxima are the Fowler-Nordheim resonances modified by the interference effect. We find that by modifying the width (or depth) of the quantum well we can destroy or enhance a given transmission resonance.

Finally we calculated the infrared absorption $\alpha(\hbar\omega)$

from the ground state in the well to the continuum of states above and we found sharp structures in $\alpha(\hbar\omega)$ corresponding to the peaks in $\Delta\rho(E)$. The absorption peaks do not show any periodic modulation and their intensity is highest for narrow wells with only one bound state. These sharp structures could be observed in the GaAs/ $\text{Al}_{1-x}\text{Ga}_x\text{As}$ multiple-quantum-well system at moderate fields (about 10 kV/cm) if the barriers are sufficiently thick (≥ 500 Å). Such measurements would supply additional information about the sample (the peak positions are sensitive to the well depth and to the electric field) and they are also important for the applications in infrared detectors.

We have not considered the interband absorption²⁸ which should also reveal structures due to resonances at energies above the top of the well. In this case absorption will be the convolution of the structures for electrons and for holes. Due to the higher mass of holes $\Delta\rho(E)$ varies more rapidly for the holes than for the electrons. The slow-modulation period is also much shorter for holes. Therefore at fairly high fields (50–100 kV/cm) we can expect to see mainly the structures due to holes. However, as we mentioned previously, the correct description of the holes requires a 4×4 (or 6×6) Luttinger Hamiltonian and our parabolic, one-band calculation only applies for $k_{\parallel}=0$. We found some interesting electroreflectance results²⁹ showing the above well structures similar to the ones we discussed here but the barriers were made of graded-gap $\text{Al}_x\text{Ga}_{1-x}\text{As}$ which complicates the simple picture we considered.

The electric-field effect on the continuum is much more pronounced than on the quasibound states. We hope that our results will stimulate some experimental effort in this area.

ACKNOWLEDGMENTS

One of us (W.T.) is grateful to Professor Franco Bassani and Professor Marcello Colocci for their hospitality and encouragement during his visit in Italy.

APPENDIX: NORMALIZATION AND THE DIPOLE MATRIX ELEMENTS FOR THE AIRY FUNCTIONS

For an arbitrary solution $u(y) = \alpha \text{Ai}(y) + \beta \text{Bi}(y)$ of the Airy equation,

$$\frac{d^2}{dy^2} u(y) = y u(y), \quad (\text{A1})$$

we can multiply both sides by du/dy and integrate by parts to obtain

$$\int_{y_a}^{y_b} dy u^2(y) = \left[y u^2 - \left(\frac{du}{dy} \right)^2 \right]_{y_a}^{y_b}. \quad (\text{A2})$$

We used this equation for normalizing our wave functions and also for the determination of the local density of states.

For the absorption calculations we needed the momentum matrix element between the ground state and the excited states. This required the evaluation of the integrals

$$\int_{y_a}^{y_b} dy u_g(y) \frac{d}{dy} u_e(y-D) = -\frac{d}{dD} \int_{y_a}^{y_b} dy u_g(y) u_e(y-D), \quad (\text{A3})$$

where $u_g(y)$ and $u_e(y)$ are two solutions of the Airy equation and, from Eq. (12),

$$D = \left[\frac{2m^* eF}{\hbar^2} \right]^{1/3} \frac{\hbar\omega}{eF}. \quad (\text{A4})$$

Here $\hbar\omega$ is the energy difference between the ground state and the excited state. The integral on the right-hand side of (A3) can be calculated from the following identity:

$$\begin{aligned} \int_{y_a}^{y_b} dy u_g(y) y u_e(y-D) &= \int_{y_a}^{y_b} dy u_g(y) (y-D) u_e(y-D) \\ &+ D \int_{y_a}^{y_b} dy u_g(y) u_e(y-D), \end{aligned} \quad (\text{A5})$$

by using the Airy equation (A1) in the first two integrals and integrating by parts. We finally obtain

$$\int_{y_a}^{y_b} dy u_g(y) u_e(y-D) = \frac{1}{D} \left[u_e(y-D) \frac{d}{dy} u_g(y) - u_g(y) \frac{d}{dy} u_e(y-D) \right]_{y_a}^{y_b}. \quad (\text{A6})$$

Equations (A3) and (A6) allow for the analytic determination of the momentum matrix element.

*Permanent address: High Pressure Research Center "Unipress," Polish Academy of Sciences, Sokołowska 29, 01-142 Warsaw, Poland.

¹G. Bastard, E. E. Mendez, L. L. Chang, and L. Esaki, *Phys. Rev. B* **28**, 3241 (1983).

²M. Matsuura and T. Kamizato, *Phys. Rev. B* **33**, 8385 (1986).

³D. Ahn and S. L. Chuang, *Phys. Rev. B* **34**, 9034 (1986).

⁴E. J. Austin and M. Jaros, *Phys. Rev. B* **31**, 5569 (1985).

⁵E. J. Austin and M. Jaros, *J. Appl. Phys.* **62**, 558 (1987).

⁶E. J. Austin and M. Jaros, *Phys. Rev. B* **38**, 6326 (1988).

⁷W. Trzeciakowski, *Phys. Rev. B* **38**, 12 493 (1988).

⁸Z. Ikonić, V. Milanović, and D. Tjapkin, *Phys. Lett. A* **126**, 52 (1987).

⁹J. P. Hagon, M. Jaros, and D. C. Herbert, *Phys. Rev. B* **40**, 6420 (1989); J. P. Hagon and M. Jaros, *ibid.* **41**, 2900 (1990).

¹⁰T. B. Bahder, J. D. Bruno, R. G. Hay, and C. A. Morrison, *Phys. Rev. B* **37**, 6256 (1988); J. D. Bruno and T. B. Bahder, *ibid.* **39**, 3659 (1989).

¹¹G. Kim and B. Arnold, *Phys. Rev. B* **38**, 3252 (1988).

¹²W. Bloss, *J. Appl. Phys.* **66**, 1240 (1989).

¹³This method has been used for the study of the double-barrier tunneling structures; see W. Trzeciakowski, D. Sahu, and T. F. George, *Phys. Rev. B* **40**, 6058 (1989).

¹⁴*Handbook of Mathematical Functions*, edited by M. Abramowitz and I. A. Stegun (National Bureau of Standards, Washington, D.C., 1964).

¹⁵A factor of 2 was missing in the formulas for $\Delta\rho(E)$ in Ref. 4.

¹⁶G. D. Sanders and K. K. Bajaj, *Phys. Rev. B* **35**, 2308 (1987).

¹⁷As we mentioned in the Introduction our results are valid in a limited energy region above the barriers (about 0.2 eV) due to the Γ - X mixing at higher energies.

¹⁸The integrals of Airy functions are easily evaluated analytically (see the Appendix).

¹⁹R. H. Fowler and L. Nordheim, *R. Soc. Proc. A* **119**, 173 (1928).

²⁰W. Bloss, *Superlatt. Microstruct.* **6**, 129 (1989).

²¹K. K. Choi, B. F. Levine, C. G. Bethea, J. Walker, and R. J. Malik, *Appl. Phys. Lett.* **50**, 1814 (1987).

²²J. Callaway, *Phys. Rev.* **130**, 549 (1963); K. Tharmalingham, *ibid.* **130**, 2204 (1963); F. Aymerich and F. Bassani, *Nuovo Cimento* **48**, 358 (1967); R. W. Koss and L. M. Lambert, *Phys. Rev. B* **5**, 1479 (1972).

²³J. Bleuse, G. Bastard, and P. Voisin, *Phys. Rev. Lett.* **60**, 220 (1988); E. E. Mendez, F. Agullo-Rueda, and J. M. Hong, *ibid.* **60**, 2426 (1988).

²⁴D. Ahn and S. L. Chuang, *Phys. Rev. B* **35**, 4149 (1987); Perng-fei Yuh and K. L. Wang, *ibid.* **38**, 8377 (1988).

²⁵The bound-free absorption for $F=0$ has been calculated by Z. Ikonić, V. Milanović, and D. Tjapkin, *Appl. Phys. Lett.* **54**, 247 (1989).

²⁶U. Ekenberg, *Phys. Rev. B* **36**, 6152 (1987); Z. Ikonić, V. Milanović, D. Tjapkin, and P. Pajević, *ibid.* **37**, 3097 (1988).

²⁷B. F. Levine, C. G. Bethea, K. K. Choi, J. Walker, and R. J. Malik, *J. Appl. Phys.* **64**, 1591 (1988); B. F. Levine, C. G. Bethea, G. Hasnain, J. Walker, and R. J. Malik, *Appl. Phys. Lett.* **53**, 296 (1988).

²⁸D. A. B. Miller, D. S. Chemla, T. C. Damen, A. C. Gossard, W. Wiegmann, T. H. Wood, and C. A. Burrus, *Phys. Rev. B* **32**, 1043 (1985).

²⁹P. C. Klipstein, P. R. Tapster, N. Apsley, D. A. Anderson, M. S. Skolnick, T. M. Kerr, and K. Woodbridge, *J. Phys. C* **19**, 857 (1986).